INTERNATIONAL JOURNAL FOR NUMERICAL AND ANALYTICAL METHODS IN GEOMECHANICS
Int. J. Numer. Anal. Meth. Geomech. 2013; **37**:1969–1986
Published online 24 July 2012 in Wiley Online Library (wileyonlinelibrary.com). DOI: 10.1002/nag.2118

Stability of earth slopes. Part I: two-dimensional analysis in closed-form

Lysandros Pantelidis[1,*,†] and D. V. Griffiths[2,3]

[1]*Department of Civil Engineering and Geomatics, Cyprus University of Technology, 3603, Lemesos, Cyprus*
[2]*Department of Civil and Environmental Engineering, Colorado School of Mines, Golden, CO 80401, U.S.A.*
[3]*Australian Research Council Centre of Excellence for Geotechnical Science and Engineering, University of Newcastle, Callaghan, NSW 2308, Australia*

SUMMARY

A closed-form solution (CFS) satisfying both equilibrium of moments and forces for the stability analysis of earth slopes in 2D is proposed. The sliding surface is assumed circular and treated as a rigid body, allowing the internal state of stress to be ignored. The proposed solution can be applied to both homogenous and non-homogenous slopes of either simple or complex geometry, and can also deal with any kind of additional loading. The method is based on the fact that, all possible forces acting on the slope can be projected onto the failure surface where they are broken into driving and resisting ones. Comparison of the safety factors obtained by the proposed CFS and those obtained by traditional limit equilibrium methods, as applied to several test examples, indicates that the proposed method is more conservative, whereas moreover, it gives a more realistic point of view for the formation of tension crack in slopes. Copyright © 2012 John Wiley & Sons, Ltd.

Received 11 May 2011; Revised 25 May 2012; Accepted 29 May 2012

KEY WORDS: slope stability; closed-form solution; lumped mass approach; 2D analysis; rigid body rotation

1. INTRODUCTION

Almost a century has passed since the failure of the Stigberg quay in the harbor of Gothenburg (5 March 1916), which became the subject of the first attempt to use 'slices' in slope stability analysis [1–3]. The analysis in question, which assumed that the slide occurred along a circular arc, resulted later in the development of the 'Swedish Slip Circle Method' (also called the $\varphi_u = 0$ method). Fellenius [4, 5] developed this method further creating a method known as the Ordinary Method of Slices or Fellenius's Method. Since then, a large number of limit equilibrium methods (LEM) have been developed, for example, [6–13]; the limit equilibrium analysis considers the ultimate limit state of the slope. In all these methods, the available number of equations of equilibrium is smaller than the number of unknowns in slope stability problems. As a result, all equilibrium methods of slope stability analysis employ assumptions to render the problem determinate (e.g., [14]). Generally, the assumptions made for the different unknown variables involved in the equilibrium equations do not result in much difference in the final factor of safety. However, as it shall be shown later on, great differences may be observed and indeed, on the unsafe side. It is noted that, in essence, the only significant difference among the different methods is the assumption made about the location and inclination of the interslice forces or the relation between the interslice normal and shear forces.

The existing LEM can be broadly classified into 'simplified' methods (e.g., Bishop simplified, Corps of Engineers, Janbu simplified/corrected, Lowe–Karafiath and Fellenius) and 'rigorous' methods (e.g., Spencer, Morgenstern-Price). The simplified methods satisfy either force or moment

*Correspondence to: L. Pantelidis, Department of Civil Engineering and Geomatics, Cyprus University of Technology, P.O. Box 50329, 3603 Lemesos, Cyprus.
†E-mail: lysandros.pantelidis@cut.ac.cy

equilibrium (not both at the same time). On the other hand, rigorous methods satisfy both force and moment equilibrium, but usually, the analysis is more tedious and may sometimes experience non-convergence problems (e.g., [15–18, 9]). Detailed comparison of limit equilibrium slope stability analysis methods have already been reported in numerous textbooks (e.g., [15, 14, 19–21]), hence, in the present paper, further reference is made only where needed.

In this paper, a closed-form 'lumped mass' approach to slope stability is proposed, in which the soil mass over a circular slip surface is considered as rigid body [9]. Thus, no assumptions are necessary regarding the internal state of stress, and the soil mass can be concentrated at its centroid as shown in Figure 1. This is in contrast to non-circular failure surfaces, which can induce significant internal stresses within the sliding volume. The fact that the internal state of stress of the sliding mass is ignored in the current work should not lead the reader to conclude that the proposed method is similar to Fellenius method, where the internal forces are erroneously ignored for the sake of simplification. When the sliding mass is divided into slices, each slice must necessarily be accompanied by consideration of lateral (inter-slice) forces corresponding to the reactions from adjacent slices. In this work, the internal forces are ignored because the whole sliding mass over the circular surface is considered as a rigid body, thus these forces do not affect the rotation. Finally, it is mentioned that it is well known that slides diverge more or less from the pure rotational pattern of failure. However, the present method includes less assumptions and thus, it could be a tool for the effective evaluation of the existing methods.

2. DEFINITION OF SAFETY FACTOR

The factor of safety for slope stability analysis is usually defined as the ratio of the ultimate shear strength divided by the mobilized shear stress at working stress levels. Although there are several ways of formulating the factor of safety FS, for the special case of circular failure studied herein, the expression of safety factor in terms of moments is the most appropriate:

$$FS_M = \frac{\text{Resisting}moments}{\text{Driving}moments} = \frac{M_f}{M_d} \tag{1}$$

where, M_f is the sum of the resisting moments and M_d is the sum of the driving moments. The center of the circle is taken as the moment point for convenience. The factor of safety is assumed to be the same at all points along the slip surface, which is typical for conventional LEM (e.g., [20]).

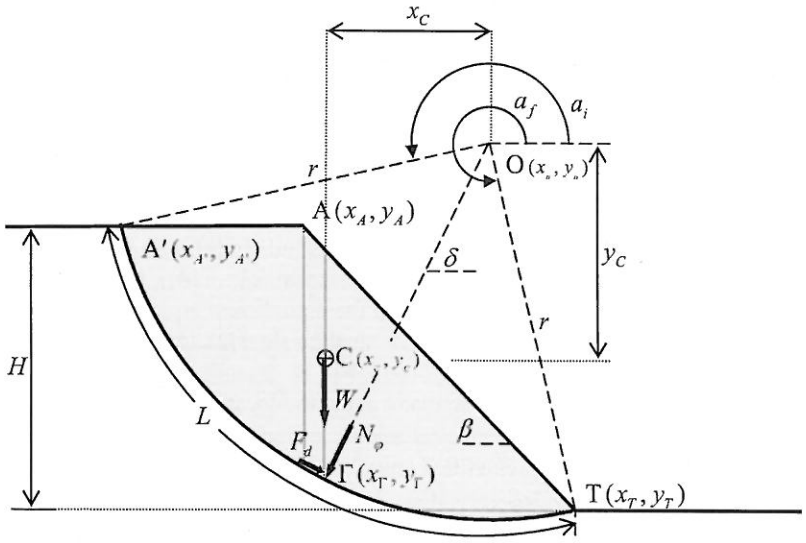

Figure 1. Example of a homogenous slope of simple geometry. The weight of the failure mass per unit length (shady area) is concentrated at the center of mass, point C. The projection of weight W intersects the slip circle at point Γ.

DOI: 10.1002/nag

3. THE PROPOSED ANALYTICAL SOLUTION

3.1. General concept

The methodology that follows is based on the fact that, at the initiation of pure rotational sliding along a circular surface, no shear forces are developed inside the failure mass. This allows internal forces to be ignored and the soil weight W above the slip surface to be idealized as a single force acting at the center of (failure) mass (Figure 1). The concentrated weighting force is then projected onto the failure surface in order for the driving and resisting moments about the center of rotation to be calculated. Similarly, other possible forces acting on the slope (e.g., pore pressures, seismic, footing, water in tension crack, etc.) can be projected onto the failure surface before calculating their moments.

Adopting Coulomb's equation, and working with effective stresses (Equation (2)), the safety factor, FS_M is given by Equation (3). The last stands for homogenous slopes in which only gravity and pore pressures act. The radius r in Equation (3) cancels out, thus, the proposed methodology satisfies force equilibrium as well. Detailed analysis of the forces included in the equation in question is given in the next section. Moreover, examples of some of the most commonly used forces in slope stability analysis are given in Section 4.

$$\tau_f = c' + (\sigma\text{-}u)\tan\varphi' = c' + \sigma\tan\varphi'\text{-}u\tan\varphi' \tag{2}$$

$$\begin{aligned} FS_M &= \frac{c'Lr + W\cos\left(\frac{\pi}{2}\text{-}\delta\right)\tan\varphi' r\text{-}\sum u\tan\varphi' r}{W\sin\left(\frac{\pi}{2}\text{-}\delta\right)r} = \\ &= \frac{c'L + W\cos\left(\frac{\pi}{2}\text{-}\delta\right)\tan\varphi'\text{-}U\tan\varphi'}{W\sin\left(\frac{\pi}{2}\text{-}\delta\right)} = FS_F \end{aligned} \tag{3}$$

The general methodology involves the extensive use of equations, which include integrals for the calculation of c', W, U and δ in Equation (3). All the integrands, however, lead to simple analytical solutions. With these equations, the proposed method leads to closed-form solution (CFS) that give the safety factor of a slope for any specific geometry and slip circle.

3.2. Forces acting on the slip surface

3.2.1. Resisting force F_c due to cohesion. The resisting force due to cohesion is simply derived by integrating cohesion, c', along the slip surface (Equation (4a)). For the homogenous slope of Figure 1, the limits of the integral in question are defined by the entry and exit points of the slip circle (points A' and T, respectively), and they are given in angular form (angle α_i and α_f, respectively). It is noted that, as the vector of the cohesion force at each point along the circular failure surface is always tangential to this surface, there is no need for the resultant cohesion force F_c to be broken into components.

$$F_C = \int_{\alpha_i}^{\alpha_f} c'\mathrm{d}s = \int_{\alpha_i}^{\alpha_f} c'r\mathrm{d}\alpha = c'r\left(\alpha_f\text{-}\alpha_i\right) \tag{4a}$$

Heterogeneity. If the slip circle meets soil layers with different cohesions, Equation (4a) is modified accordingly. For example, for the non-homogenous slope of Figure 2, the cohesion force is:

$$F_C = c'_I r(\alpha_2\text{-}\alpha_1) + c'_{II} r(\alpha_6\text{-}\alpha_2) \tag{4b}$$

DOI: 10.1002/nag

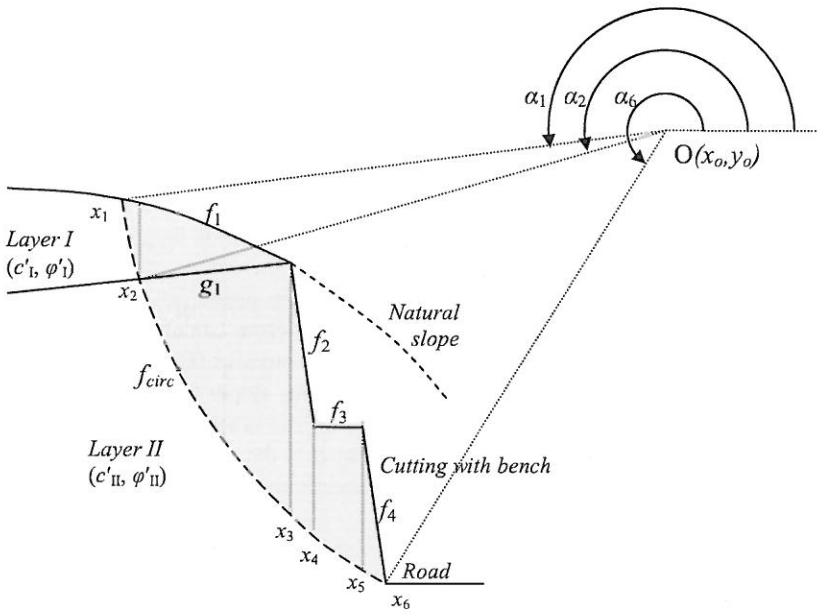

Figure 2. Example of a heterogeneous slope with complex geometry. The sliding mass is divided into six (homogenous) parts by an interlayer line (represented by function g_1) and a number of vertical lines passing through points x_1–x_6. The free ground surface consists of four parts represented by functions f_1–f_4. The failure surface crosses two soil layers.

3.2.2. Resisting friction and driving forces, F_φ and F_d respectively. In this case, the weight, W of the failure mass, as well as the x-coordinate of its center of mass, x_C, must be known. The gravity force corresponds to the weight of the area per meter depth (it refers to the third dimension), enclosed between the failure surface and the free ground surface (Figure 1, shady area). The method can be used in homogenous and non-homogenous slopes and in either simple or complex geometries following these steps (Figures 1 and 2):

(1) The free ground surface is divided into n parts, such that each one of them can be represented by a (simple) function $y=f_i(x)$, $i=1,2,\ldots,n$. The use of polynomial functions is suggested on account of their simplicity and because they can effectively represent almost any slope profile. However, any other reasonable function type could be used provided that its integral can be obtained analytically.
(2) If there are $m+1$ soil layers of different unit weight and/or shear strength values, each interface line between two layers in contact is represented by a (polynomial) function $y=g_i(x)$, $i=1,2,\ldots,m$.
(3) The failure mass is divided into q homogenous parts encompassed by an upper and a lower function, that is, $f_i(x)$ and $g_i(x)$ or $f_i(x)$ and $f_{\text{circ}}(x)$ or $g_i(x)$ and $f_{\text{circ}}(x)$ and two lateral boundaries in the form of $y=x_i$.
(4) The gravity force W, and the x-coordinate of the center of the mass x_C, are given by Equations (5) and (6), respectively. The equations in question refer to the specific homogenous slope shown in Figure 1(a). For other cases, they should be modified as needed.

$$W = \int_{x_{A'}}^{x_A} \gamma_s \{f_{A'A}(x) - f_{\text{circ}}(x)\}\,dx + \int_{x_{A'}}^{x_T} \gamma_s \{f_{AT}(x) - f_{\text{circ}}(x)\}\,dx \tag{5}$$

$$x_C = \frac{\text{total moments}}{\text{total weight}} = \frac{\int_{x_{A'}}^{x_A} \gamma_s x\{f_{A'A}(x) - f_{\text{circ}}(x)\}\,dx + \int_{x_{A'}}^{x_T} \gamma_s x\{f_{AT}(x) - f_{\text{circ}}(x)\}\,dx}{W} \tag{6}$$

DOI: 10.1002/nag

The procedure continues with the vertical projection of the force W onto the failure surface, where it is broken into two components, one tangential (F_d) and one normal (N_φ). The first one is the driving force due to gravity (Equation (3)), whereas the second one is multiplied by the friction coefficient, $\tan\varphi'$, to give the total friction force F_φ that corresponds to the product $\sigma'\tan\varphi'$ (in stress term) from Equation (2). Hence,

$$F_d = W\sin(^{\pi}/_{2}\text{-}\delta) \tag{7}$$

$$F_\varphi = N_\varphi\tan\varphi' = W\cos(^{\pi}/_{2}\text{-}\delta)\tan\varphi' \tag{8}$$

where, from Figure 1(a), $\delta = \tan^{-1}(y_\Gamma/x_\Gamma)$.

This procedure involves a major assumption regarding the point of action of F_d and N_φ, which is considered to be the same as the point of action of W on the slip surface. From a historical perspective, it is noted that this assumption is commonly used by various Methods of Slices (MoS). As shown in the Appendix, where a more rigorous approach is presented, the assumption made herein is not true; however, it always leads to the same factor of safety as that obtained using the rigorous approach. Thus, due to its simplicity, the assumption is adopted and the two components of W on the slip surface (F_d *and* N_φ) can be considered representative of the resultant normal and driving forces of the failure mass.

Heterogeneity. If the slip circle meets k soil layers with different friction angles φ'_k, then, k driving and friction forces must be calculated. Each pair of forces corresponds to the mass above the part/length of the slip circle that has the same φ'. For example, in the two-layer system of Figure 2, one pair of forces should be calculated for $x=x_1$ to $x=x_2$ and one for the rest going from $x=x_2$ to $x=x_6$.

It is apparent that in case of heterogeneous slopes, the sliding mass is divided vertically into parts (k parts for a $k-$layer system). Although the present analytical solution ignores the inter-part forces (essentially a term equivalent to the 'interslice forces'), as the number of interfaces created in the analysis is small ($k-1$ interfaces for a $k-$layer system), the error in the safety factor value is minor. A relevant example of a homogenous slope divided into two parts is given at the end of Section 5. It may be noted that in the case of various MoS, where the number of slices is very small, the main source of error is due to the fact that the failure surface is represented by a coarse polygonal path, something that is avoided by the present method where the circular surface is strictly retained. On the other hand, if the number of slices in a method of slices is great enough for the failure surface to be closely represented by a smooth polygonal path, the error in the safety factor value is mainly due to the assumptions made for the interslice forces. However, even if the Fellenius method is used where interslice forces are completely ignored, the safety factor values are usually close to the ones obtained by more rigorous methods (e.g., Bishop [6], Janbu [7] or Morgenstern-Price [9] method).

3.2.3. Pore pressure force F_w. The pore pressure distribution is shown in Figure 3 with dotted line (function $u(x)$). The resultant pore pressure force U can be calculated according to Equation (9a), as the area bounded between this line and the circular failure surface. However, as γ_w is constant, it is more convenient for U to be calculated directly from the area between the free water surface and the slip surface, where all functions are already known according to Equation (9b).

$$U = \int_{x_{B'}}^{x_\Gamma}\{u(x)\text{-}\gamma_w f_{\text{circ}}(x)\}\,dx = \int_{x_{B'}}^{x_\Gamma}\{\gamma_w h_w(x)\text{-}\gamma_w f_{\text{circ}}(x)\}\,dx \tag{9a}$$

$$U = \gamma_w A_w = \gamma_w\left[\int_{x_{B'}}^{x_B}\{f_{B'B}(x)\text{-}f_{\text{circ}}(x)\}\,dx + \int_{x_B}^{x_T}\{f_{BT}(x)\text{-}f_{\text{circ}}(x)\}\,dx\right] \tag{9b}$$

The buoyancy force U, which acts radially on the slip surface, is multiplied directly by the friction coefficient, $\tan\varphi'$ giving the force F_u that corresponds to the term $u\tan\varphi'$ in the Coulomb equation (Equation 2), that is,

$$F_u = U\tan\varphi' \tag{10}$$

DOI: 10.1002/nag

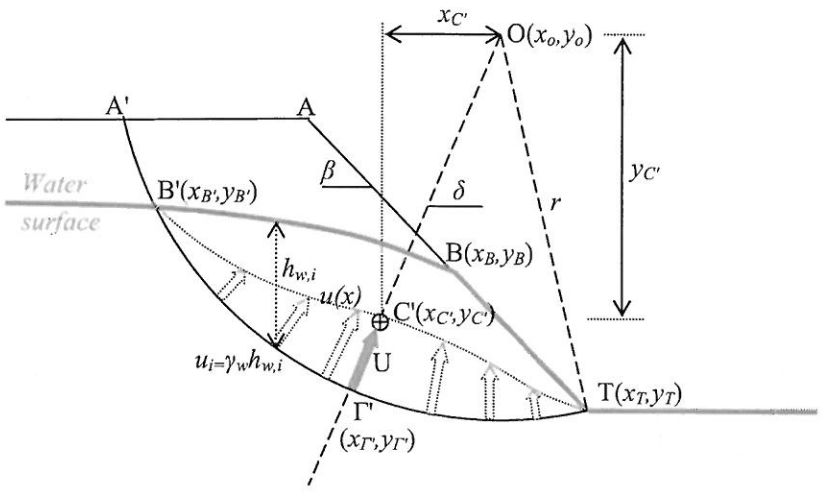

Figure 3. Example: Line of action on the slip surface of the resultant pore pressure force; C′ is the centroid of the area bounded by the water surface and the slip circle. The pore pressure at a given point i along the slip surface equals $u_i = \gamma_w h_{w,i}$.

For information purposes, it is noted that, U acts at the intersection point between the radius passing through the centroid C′ of the area bounded between the free water surface and the slip surface (point Γ′, Figure 3). The coordinates of point C′ are as follows:

$$x_{C'} = \frac{\text{total moments}}{\text{total weight}} = \frac{\int_{x_{B'}}^{x_B} \gamma_w x\{f_{B'B}(x) - f_{\text{circ}}(x)\}\,dx + \int_{x_B}^{x_T} \gamma_w x\{f_{BT}(x) - f_{\text{circ}}(x)\}\,dx}{U} \tag{11a}$$

$$y_{C'} = \frac{\textit{total moments}}{\textit{total weight}} = \frac{\int_{y_{B'}}^{y_B} \gamma_w y\{f_{B'B}(y) - f_{circ}(y)\}dy + \int_{y_B}^{y_T} \gamma_w y\{f_{BT}(y) - f_{circ}(y)\}dy}{U} \tag{11b}$$

4. EXTERNAL FORCES ACTING ON THE SLOPE

The methodology described is easily generalized to include other types of external forces commonly encountered in slope stability analysis. Some of these load cases are shown in Figure 4 and include water-filled tension crack, pseudo-static earthquake loading (horizontal and vertical components) and footing loading on the crest of the slope or elsewhere and pool loading due to free-standing water adjacent to the slope. As a general rule, additional forces of this type are projected onto the slip surface and broken into normal and tangential components. Each normal component is multiplied by both the coefficient of friction $\tan\varphi'$ and the slip circle radius r and then added to the numerator of the safety factor equation (Equation 3). The tangential component is multiplied only by the radius r, before it is added to the denominator of the safety factor equation.

Some additional comments are given as follows:

- *Heterogeneity*: If the slip circle meets various soil layers of different friction angle φ', then, the normal component of each weighing force W_i is multiplied by the respective coefficient of friction $\tan\varphi_i'$ (Figure 5(a)). The same goes for the pore water pressures, where the distribution function $u(x)$ is divided into parts in a manner similar to the one applied to W_i (vertical division). Each one of these parts is multiplied by the respective coefficient of friction.
- *Tension crack*: The tension crack is taken into account by simply changing in Equation (5) the boundary $x_{A'}$ (entry point, Figure 1) with the x −coordinate of the location of the tension crack, $x_{A''}$ (entry point, Figure 4). Conservatively, it is assumed that the soil has no tensile strength.
- *Water in tension crack*: This distribution is triangular as shown in Figure 4, and the resultant force V acts perpendicularly to the tension crack wall at one third of the height of water. As the force

DOI: 10.1002/nag

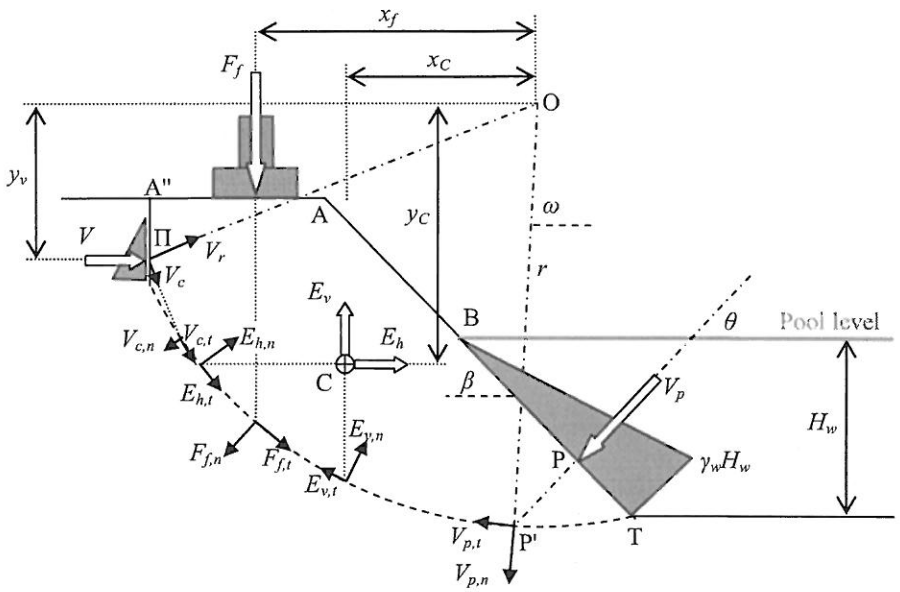

Figure 4. Example: Possible external forces acting on a homogenous earth slope (see Figures 1 and 2 for more details about gravity force and pore pressures).

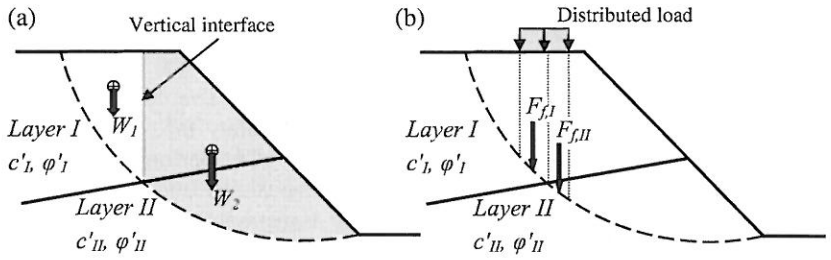

Figure 5. Non-homogeneous slopes: (a) vertical division of sliding mass and (b) division of distributed load.

V cannot directly be projected onto the failure surface, but gives moment as for the center of rotation, it is broken into two components, a radial and a perpendicular to the radial component (V_r and V_c, respectively). The first one gives neither moment (as for the center of rotation, O) nor friction force, thus, it can be neglected. The second one is projected onto the failure surface, where it is broken into a tangential and a normal component ($V_{c,t}$ and $V_{c,n}$, respectively). It is noted that, the force $V_{c,t}$ produces equal moment as for the point O comparing with the respective one of its mother force V, that is, $Vy_v = V_c(O\,II) = V_{c,t}r$. Moreover, as it shown in Figure 4, the force V contributes to the friction along the slip surface through the normal component $_?V_{c,n}$; however, this contribution is rather minor.

- *Seismic force*: Pseudo-static seismic forces act at the center of the (sliding) mass, and can be applied directly in homogenous earth slopes as shown in Figure 4. The direction of the components of seismic force (horizontal and vertical), are also indicated. An additional step is needed if the slip surface crosses more than one layers (e.g. see Figure 6) where the failure mass should be divided by *horizontal* and/or *vertical* lines (boundaries) passing through the points on the slip surface where φ' changes. For every sub-area that arises from the division, both the magnitude of earthquake forces and the coordinates of each center of mass must be calculated. Following this, each gravity force is then multiplied by the required seismic coefficient. Finally, the forces are projected onto the slip surface and broken into normal and tangential component as described previously.
- *Pool loading*: This distribution is triangular as shown in Figure 4, and the resultant force V_p acts perpendicularly to the slope face at one third of the vertical height of the water above the slope toe.

DOI: 10.1002/nag

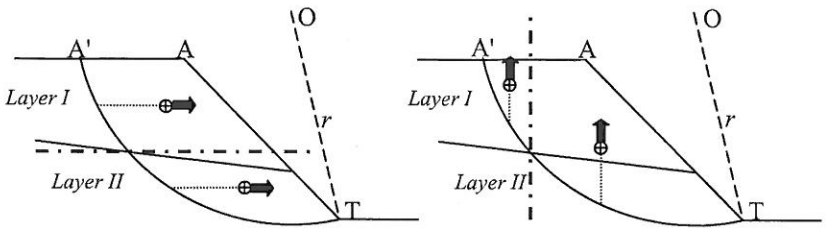

Figure 6. Horizontal and vertical seismic forces in a two-layer system.

- *Distributed loadings in non-homogenous slopes*: If the projection of a distributed load (e.g., footing, pool loading) on the slip surface meets more than one soil layers, that is, more than one φ' values, then the distributed loading should be broken into parts having as division criterion the change of angle φ' (e.g., Figure 5(b)).

5. EXAMPLES

Two examples of the proposed CFS, one referring to a homogenous slope and one to a non-homogenous slope (Figure 7(a) and (b), respectively), are presented. A third example refers to a homogenous slope consisting of two layers of the same material to show the influence on the safety factor of neglecting the inter-part forces after dividing the slope into two parts.

Additional loading, such as pore water pressures, footing on the crest and pool loading, have been included. The results obtained by the proposed method and four of the most familiar LEM[1] are summarized in Table I (column I and columns II–V, respectively). The deviation values (minimum and maximum) in the same table are given in relation to the safety factor values obtained by the proposed CFS. All solutions with the proposed method have been performed on an Excel™ (MS Office™) spreadsheet, where, in addition, it is noted that the *Solver* add-in was used to minimize the objective function for the factor of safety given by Equation (3) (modified as necessary for different loading cases and stratification). The optimization parameters were given as the center coordinates (x_o, y_o), the circle radius r, and the x–coordinate of the tension crack (entry point at $x_{A''}$). The optimized parameters of the critical slip circle, as found for each example using the proposed method, are presented in Table II.

Homogenous slope (*Figure* 7(*a*)): The slope has height $H = 10$m and gradient $\tan\beta = 1:1$. The characteristics of the soil material are as follows: $c' = 20$kPa, $\varphi' = 31°$ and $\gamma_s = 20$kN/m^3. In Table I, case 1a considers only the gravitational force of slope. In case 1b, the solutions were performed allowing the various methods to take into account possible formation of tension crack. A horizontal water table height $H_w = 3$m above the slope toe within the soil is assumed in case 1c (Table I) continuing downstream along the soil surface profile. In Case 1d (Table I), the water table has been extended outside the slope to include pool loading. In cases 1e and 1f, the soil is considered dry (no pore water pressures), whereas vertical point loads (200 and 50 kN, respectively) have been applied near the crest (horizontal distance from slope toe and slope crest 11 and 1 m, respectively).

Non-homogenous slope (*Figure* (7*b*)): The two-layer slope has a total height $H = 7.5$m and gradient $\tan\beta = 1.5:1$. The soil characteristics of the upper layer (Layer I) are: $c'_I = 20$kPa, $\varphi'_I = 31°$ and $\gamma_{s,I} = 20$kN/m^3, and of the lower layer (Layer II): $c'_{II} = 15$kPa, $\varphi'_{II} = 25°$ and $\gamma_{s,II} = 16$kN/m^3. The thickness of Layer I is 3.5 m, whereas Layer II has infinite depth ($h = 4$m for Layer II if measured from slope toe). Case 2a (Table I) considers only the gravitational force of slope. In addition to the gravitational force, cases 2b and 2c assume horizontal water table at height $H_w = 4$ and 2 m, respectively, above the slope toe. In case 2d, the water table is 2 m above slope toe, and it is extended outside the slope to include pool loading. In cases 2e and 2f the soil is considered dry (no pore water pressures), whereas

[1]LEM solutions were obtained using the package Slide™.

DOI: 10.1002/nag

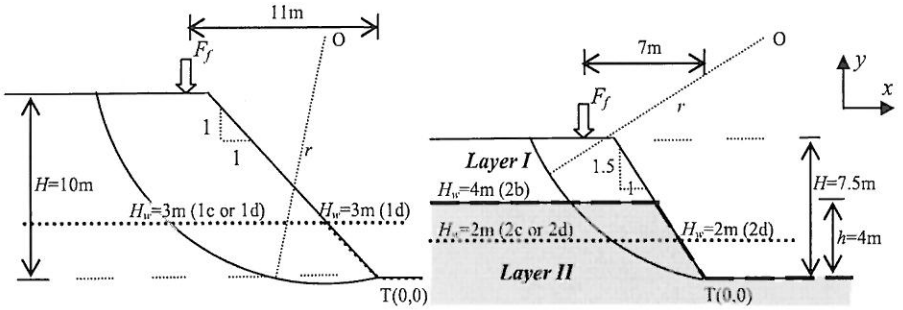

a) Homogenous slope b) Non-homogenous slope

Figure 7. Application examples. Cases 1a and 2a refer to the gravitational force only, whereas in case 1b, tension crack was allowed to be developed. Text in brackets following the notation of water table height (H_w) indicates other loading cases (see also Table I).

vertical point loads (200 and 50 kN, respectively) have been applied near the crest (horizontal distance from slope toe and slope crest 7 and 2 m, respectively).

An important outcome from Table I is that, in some cases, the deviation between the safety factor obtained by the proposed CFS and the different MoS can be very high, either on the safe or unsafe side. For the limited number of examples shown in the table in question, the deviations range from −12.4% (safe side) to 29.1% (unsafe side).

Homogenous slope consisting of two layers of the same material: Consider the 7.5-m high slope with gradient 1.5 V:1 H of Figure 7(b). The slope, here, consists also of two horizontal soil layers, but of the same characteristics. Two material cases have been considered, case 3a with $c' = 20$ kPa, $\varphi' = 31°$ and $\gamma_s = 20\text{kN/m}^3$ and case 3b with $c' = 15\text{kPa}$, $\varphi' = 25°$ and $\gamma_s = 16\text{kN/m}^3$. The height h of the underlain layer is considered variable and ranges from $h = 0$ to $h = H = 7.5\text{m}$ allowing the study of the influence of h on the safety factor. For comparison purposes, the center and the radius of rotation have been kept constant ($x_o = 1.795$ m, $y_o = 9.645$ m and $R = 9.810\text{m}$). It is apparent that these values do not reflect a minimum safety factor value, but this is not the point herein. As shown in the diagram of Figure 8, the safety factor value is influenced by the location of the vertical interface that passes through the intersection point between the slip circle and the line dividing the soil mass into two layers of the same material (see also Figure 5(a)). However, neglecting the inter-part forces acting on the vertical interface results to a minor error in safety factor, which is generally up to 1% or a little higher. It is remarkable that the two curves are almost parallel to each other and that they present minimum for the same h value. Finally, it is reminded that if the proposed method is applied to a stratified slope with $k$strata, only the internal forces acting on $k-1$ interfaces are ignored (usually $k-1=1$ or 2; for homogenous slopes, $k-1=0$) in contrast to Fellenius method where the internal forces of $n-1$ interfaces are ignored (where n is the number of slices used).

In addition to these, 20 other examples are given aiming at a more objective and integrated comparison of the proposed method with some of the most well known and commonly used MoS in practice. The soil and geometric characteristics of slopes are given in Table III, whereas the safety factor values are shown in Table IV; values in gray shade indicates that the critical failure surface involves the formation of tension crack (such formation was free to be developed in all solutions). For comparison reasons, the safety factor of slopes obtained by using the proposed method without the formation of tension crack is also given (see column II in Table IV). The safety factor deviations are given in Table V. All slopes are considered dry, and moreover, where tension cracks have been developed in the solutions, these are free from water. The 20 highway slopes that were chosen can be considered representative to give quite secure conclusions, as they cover a wide range of soil types and slope geometries; height, 3–20 m; inclination angles, 32°–68°. All the examples except for the 11th, which refers to a slope at Mount Cronos (Ancient Olympia), refer to slopes of the wider area of North Greece. It is worth mentioning that the first 10 slopes consist of the same soil

DOI: 10.1002/nag

Table I. Application examples.

Case #	Loading case	I	II	III	VI	V	Deviation	
		CFS	OMS	Bish Simp.	Spen.	M–P(Sine)	Min (%)	Max (%)
1a	Gravitational force only	1.609	1.569	1.633	1.628	1.627	−2.5	1.5
1b	As 1a; tension crack is considered	1.555	1.569	1.633	1.628	1.627	0.9	5.0
1c	As 1a plus pore pressures ($H_w = 3$ m, constant)	1.468	1.406	1.460	1.461	1.458	−4.2	−0.5
1d	As 1c plus pool loading ($H_w = 3$ m)	1.681	1.525	1.622	1.620	1.617	−9.3	−3.5
1e	As 1a plus point load 200 kN at $(x,y)=(-11,10)$	1.268	1.111	1.306	1.262	1.269	−12.4	3.0
1f	As 1a plus point load 50 kN at $(x,y)=(-11,10)$	1.487	1.444	1.541	1.530	1.529	−2.9	3.6
2a	Gravitational force only	1.317	1.304	1.289	1.339	1.335	−2.1	1.7
2b	As 2a plus pore pressures ($H_w = 4$ m, constant)	1.117	1.059	0.988	1.193	1.192	−11.5	6.8
2c	As 2a plus pore pressures ($H_w = 2$ m, constant)	1.243	1.221	1.174	1.319	1.309	−5.6	6.1
2d	As 2c plus pool loading ($H_w = 2$ m)	1.357	1.298	1.292	1.334	1.337	−4.8	−1.5
2e	As 2a plus point load 200 kN at $(x,y)=(-7.0,7.5)$	0.739	0.754	0.954	0.882	0.896	2.0	29.1
2f	As 2a plus point load 50 kN at $(x,y)=(-7.0,7.5)$	1.107	1.099	1.178	1.161	1.164	−0.7	6.4

CFS = proposed closed-form solution; OMS: Ordinary Method of Slices/Fellenious; Bish.(simp.) = Bishop (simplified); Spen. = Spencer; and M–P(Sine) = Morgenstern–Price (sine function for line of thrust). Deviation (%) = $100(1-F_{PG}/F_{MoS})$.

DOI: 10.1002/nag

Table II. Radius and coordinates of the center of the critical slip circle for the examples presented in Table I.

Case #	x_o	y_o	r	x_{tc}	Case #	x_o	y_o	r
1a	1.335	14.886	14.946	n/a	2a	1.795	9.645	9.810
1b	1.185	14.237	14.287	−11.587	2b	0.811	8.565	8.604
1c	1.158	14.576	14.622	n/a	2c	1.181	8.923	9.001
1d	1.283	14.877	14.932	n/a	2d	0.780	8.979	9.012
1e	8.934	20.878	22.709	n/a	2e	0.781	7.746	7.785
1f	1.273	12.450	12.515	n/a	2f	1.296	8.226	8.328

x_{tc} = x-coordinate of the tension crack.

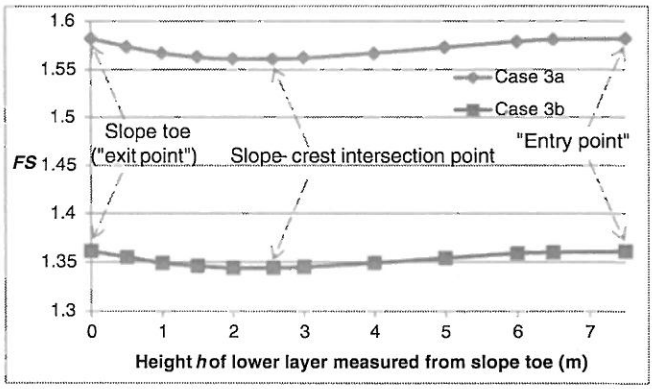

Figure 8. Example of homogenous slope consisting of two layers of the same material: Influence of the location of the vertical interface dividing the slip mass into two parts on the safety factor.

Table III. Comparison examples: Soil and geometric characteristics of slopes.

# of example	c' (kPa)	φ' (°)	γ (kN/m^3)	H (m)	tan β
1	47	35	20	3.0	2.500
2	47	35	20	5.3	2.500
3	47	35	20	15	2.500
4	47	35	20	9.0	2.000
5	47	35	20	9.0	1.000
6	47	35	20	6.2	1.500
7	47	35	20	4.6	1.500
8	47	35	20	4.3	1.500
9	47	35	20	9.1	1.500
10	47	35	20	19.5	2.500
11	5	32	21	10.0	0.625
12	20	31	20	9.0	1.327
13	0.1	36	18.5	16.5	0.543
14	15	34	21	5.0	1.000
15	22	28	17.5	6.5	1.150
16	22	28	17.5	6.0	1.111
17	22	28	17.5	5.6	1.376
18	20	32	20	3.3	1.036
19	20	28	18	5.8	1.235
20	20	28	18	3.9	1.235

material, whereas the distance between the first and the last on the road is less than 2 km. This allows for focusing on the slope geometry.

From Tables IV and V, it is inferred that

- In the great majority of cases, the factor of safety derived from the proposed method lies below those obtained by using the different MoS with deviations ranging from −3% (safe side) to 51% (unsafe side).

DOI: 10.1002/nag

Table IV. Comparison examples: Safety factors of slopes.

	I	II	III	IV	V	VI	VII	VIII	IX	X	XI
Example #	CFS Ten.cr.	CFS No t.c.	OMS	Bish. Simp.	Janbu Simp.	Janbu Corr.	Spen.	CE #1	CE #2	L–K	M–P Sine
1	4.052	4.833	4.666	4.523	5.060	5.260	5.134	6.021	6.101	4.973	5.062
2	2.665	3.111	2.992	2.925	3.222	3.340	3.341	3.304	3.377	3.181	3.283
3	1.403	1.567	1.513	1.513	1.527	1.629	1.548	1.589	1.616	1.552	1.540
4	2.039	2.282	2.232	2.212	2.296	2.411	2.457	2.325	2.379	2.324	2.317
5	2.720	2.877	2.828	2.896	2.819	2.992	2.895	2.972	3.051	2.966	2.892
6	2.879	3.185	3.147	3.146	3.208	3.383	3.267	3.246	3.367	3.215	3.266
7	3.527	3.941	3.907	3.894	4.000	4.215	4.178	4.111	4.237	4.034	4.106
8	3.700	4.143	4.105	4.093	4.209	4.431	4.401	4.395	4.514	4.224	4.386
9	2.265	2.472	2.441	2.449	2.471	2.598	2.471	2.472	2.591	2.481	2.471
10	1.223	1.350	1.308	1.315	1.321	1.403	1.336	1.366	1.389	1.345	1.331
11	1.392	1.396	1.362	1.425	1.352	1.422	1.422	1.428	1.433	1.426	1.422
12	1.417	1.501	1.466	1.501	1.467	1.546	1.500	1.526	1.558	1.527	1.498
13	1.362	1.362	1.360	1.365	1.360	1.379	1.365	1.365	1.365	1.365	1.365
14	1.949	2.029	1.982	2.055	1.967	2.088	2.051	2.091	2.132	2.087	2.048
15	1.912	2.041	2.005	2.043	2.012	2.131	2.045	2.064	2.156	2.088	2.042
16	2.033	2.171	2.133	2.175	2.139	2.268	2.176	2.178	2.299	2.190	2.173
17	1.934	2.105	2.076	2.091	2.101	2.216	2.100	2.100	2.216	2.114	2.100
18	2.800	2.987	2.935	2.993	2.942	3.125	2.996	3.024	3.177	3.028	2.992
19	1.842	1.977	1.945	1.975	1.957	2.069	1.970	1.970	2.084	1.985	1.975
20	2.349	2.553	2.519	2.543	2.547	2.695	2.547	2.548	2.711	2.561	2.547

CFS = proposed closed-form solution; OMS: Ordinarry Method of Slices; Bish. = Bishop; Spen. = Spencer; CE = Corps of Engineers; L–K = Lowe–Karafiath; and M–P = Morgenstern–Price.

Table V. Comparison examples: Deviation of safety factors of slopes. Dev (%) = $(FS_n\ FS_I - 1)100$, where n = II. . .XI (number of column; see Table IV). FS_I refers to the first column of Table IV.

	I	II	III	IV	V	VI	VII	VIII	IX	X	XI	Min	Max
Example #	CFS t.c.	CFS No t.c.	OMS	Bish. Simp.	Janbu Simp.	Janbu Corr.	Spen.	CE #1	CE #2	L–K	M–P Sine		
1	0	19	15	12	25	30	27	49	51	23	25	12	51
2	0	17	12	10	21	25	25	24	27	19	23	10	27
3	0	12	8	8	9	16	10	13	15	11	10	8	16
4	0	12	9	8	13	18	21	14	17	14	14	8	21
5	0	6	4	6	4	10	6	9	12	9	6	4	12
6	0	11	9	9	11	18	13	13	17	12	13	9	18
7	0	12	11	10	13	20	18	17	20	14	16	10	20
8	0	12	11	11	14	20	19	19	22	14	19	11	22
9	0	9	8	8	9	15	9	9	14	10	9	8	15
10	0	10	7	8	8	15	9	12	14	10	9	7	15
11	0	0	−2	2	−3	2	2	3	3	2	2	−3	+3
12	0	6	3	6	4	9	6	8	10	8	6	3	10
13	0	0	0	0	0	1	0	0	0	0	0	0	1
14	0	4	2	5	1	7	5	7	9	7	5	1	9
15	0	7	5	7	5	11	7	8	13	9	7	5	13
16	0	7	5	7	5	12	7	7	13	8	7	5	13
17	0	9	7	8	9	15	9	9	15	9	9	7	15
18	0	7	5	7	5	12	7	8	13	8	7	5	13
19	0	7	6	7	6	12	7	7	13	8	7	6	13
20	0	9	7	8	8	15	8	8	15	9	8	7	15
min	0	0	−1	0	−3	1	0	0	0	0	0		
max	0	19	15	12	25	30	27	49	51	23	25		

CFS = proposed closed-form solution; OMS: Ordinarry Method of Slices; Bish. = Bishop; Spen. = Spencer; CE = Corps of Engineers; L–K = Lowe–Karafiath; and M–P = Morgenstern–Price.

DOI: 10.1002/nag

- The higher the factor of safety, the greater the deviation in safety factor.
- Comparing only the results obtained by using the different MoS (the proposed method has been ignored here), it is noted that the deviations may also be quite high for the same example ranging, generally, from −5% to 35%; Bishop's simplified method was taken as point of origin. Having as point of origin the Morgenstern–Price's method the deviation ranges between −11% and 21%. The deviation from the unsafe side is too high and considering that these 20 examples do not include water or other loadings, the existing methods raise serious queries about their effectiveness.
- Allowing the formation of tension crack in all methods, the method that gives the most conservative safety factor values is the proposed one (Table IV, column I).
- In most of the cases, the different MoS resulted to slip surface without the formation of tension crack. Using the proposed method, on the other hand, the minimum safety factor generally corresponds to a failure surface with tension crack, although, in some cases the difference is only minor as the tension crack appears very close to the entry point of slip circle.
- Among the various MoS, the Ordinary Method of Slices and Bishop's method are the most conservative.
- In the majority of cases, the Janbu (corrected) and the Corps of Engineers (CE #1 and CE #2) methods are the least conservative. The two Corps of Engineers methods gave some of the safety factors with the greatest deviation (see Table IV and V, first example) and indeed on the unsafe side.
- Generally, it is observed that the shorter the slope and the higher the cohesion are, the greater the deviation in safety factor is.
- A tension crack may reduce the safety factor of slopes by as much as 19% (and apparently more), even if it is not filled with water.
- The influence on the safety factor of slopes depends on the soil and geometric characteristics of slopes.
- In the existing limit equilibrium software, the location/depth of tension crack is either related to the operator of the normal force at the slice base, which means that it is strongly influenced by the assumptions made regarding the interslice forces, or it is defined in terms of Rankine's active earth pressure theory using Equation (12). The second approach not only refers exclusively to homogenous slopes but moreover, it does not take into consideration the geometry of slope and pore pressures. In the proposed method, the tension crack cuts the slope in the transition point along the failure surface between tension and compression.

$$z_c = \frac{2c'}{\gamma} \tan\left(\frac{\pi}{4} + \frac{\varphi'}{2}\right) \tag{12}$$

6. SUMMARY AND CONCLUDING REMARKS

Over the last 80 years, a large number of LEM have been proposed for the stability analysis of earth slopes against circular and non-circular failure based on MoS. The division of a slope into slices however, renders the problem statically indeterminate, and assumptions are inevitably necessary regarding interslice forces.

The proposed CFS treats the sliding mass as a rigid body, thus the problem becomes statically determinate, and a solution can be found without needing to know the internal stress state within the failure mass. The method can be applied to non-homogenous slopes with complex geometry together with various kinds of external loading. The method is also able to determine the critical location of tension crack by simply varying the entry point of the slip circle. The implementation of the procedure is simple and can be carried out on commonly available spreadsheet software. Comparison of the safety factors obtained by using the proposed method and the ones obtained by using the traditional LEM, as applied to several test examples, indicates that the proposed method is more conservative, whereas moreover, it gives a more realistic point of view for the formation of tension crack in slopes. The last is, generally, a weak point of all the existing LEM.

DOI: 10.1002/nag

APPENDIX

In this Appendix, the magnitude and point of action of the resultant normal and driving force due to the weight of the sliding mass is calculated by integrating along the slip surface. First, the sliding mass is divided in the limit as the slice widths tend to zero resulting in an infinite number of vertical slices. As the sliding mass is examined as a whole, the interslice forces (E_i *and* X_i) cancel out and therefore, for the sake of brevity, they are ignored. The weight of each slice W_i is broken into two components, one normal $N_{\varphi,i}$ and one tangential $F_{d,i}$ to the base (Figure 9); the integration along the slip surface of these forces will finally give the resultant normal and driving force respectively. It should be emphasized that the force $N_{\varphi,i}$ is not the normal reaction at the base of the slice, the magnitude of which is affected by the interslice forces. As each one of the $N_{\varphi,i}$ *and* $F_{d,i}$ forces has its own direction, it is necessary that both be analyzed into the $x-$direction *and* $y-$direction; that is, $(N_{x,i}, N_{y,i})$ and $(F_{x,i}, F_{y,i})$, respectively.

Therefore, the magnitude of the two components of the resultant normal force (Figure 10) are as follows:

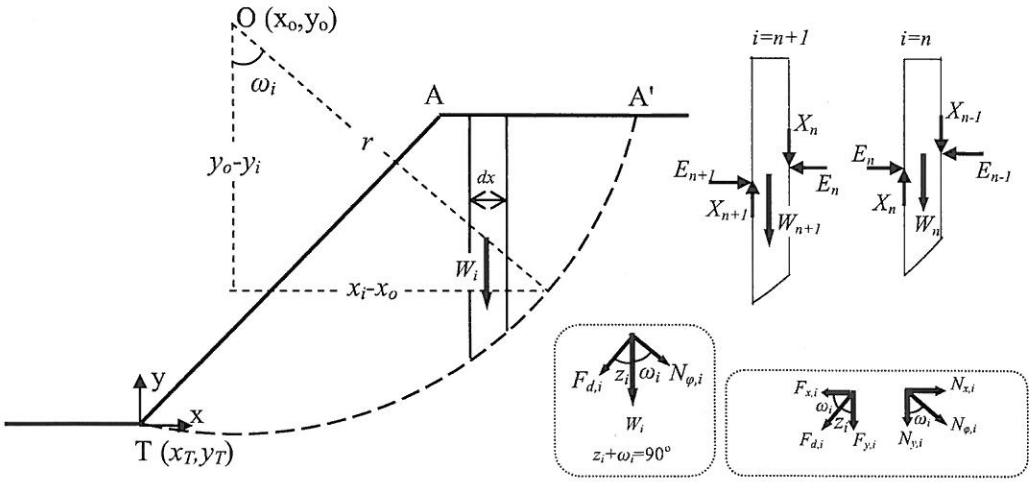

Figure 9. The sliding mass divided into an infinite number of vertical slices.

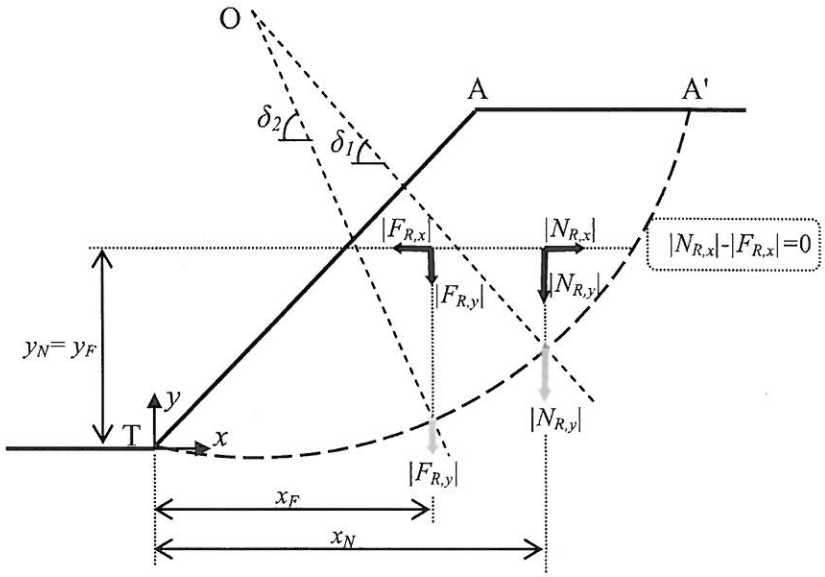

Figure 10. Resultant normal and driving forces and their points of action.

DOI: 10.1002/nag

$$N_{R,x} = + \int N_{x,i} \mathrm{d}y = + \int N_i \sin \omega_i \mathrm{d}y = \\ = + \int W_i(y) \sin \omega_i \cos \omega_i \mathrm{d}y \tag{A.1}$$

$$N_{R,y} = - \int N_{y,i} \mathrm{d}x = - \int N_i \cos \omega_i \mathrm{d}x = \\ = - \int W_i(x) \cos^2 \omega_i \mathrm{d}x \tag{A.2}$$

Similarly, the magnitude of the two components of the resultant driving force (Figure 10) are the following:

$$F_{R,x} = - \int F_{x,i} \mathrm{d}y = - \int F_{d,i} \cos \omega_i \mathrm{d}y = \\ = - \int W_i(y) \sin \omega_i \cos \omega_i \mathrm{d}y \tag{A.3}$$

$$F_{R,y} = - \int F_{y,i} \mathrm{d}x = - \int F_{d,i} \sin \omega_i \mathrm{d}x \\ = - \int W_i(x) \sin^2 \omega_i \mathrm{d}x = \\ = - \int W_i(x)(1 - \cos^2 \omega_i) \mathrm{d}x \tag{A.4}$$

where,

$$\sin \omega_i \cos \omega_i = \frac{x - x_o}{r} \cdot \frac{y_o - y}{r} = \frac{\sqrt{r^2 - (y_o - y)^2}(y_o - y)}{r^2} \tag{A.5}$$

$$\cos^2 \omega_i = 1 - \sin^2 \omega_i = 1 - \left(\frac{x - x_o}{r}\right)^2 \tag{A.6}$$

$$W_i(x) = \gamma_s \{f_i(x) - f_{\mathrm{circ}}(x)\} \tag{A.7}$$

$$W_i(y) = \gamma_s \{f_i(y) - f_{\mathrm{circ}}(y)\} \tag{A.8}$$

The operators in front of the integrals (Equations (A.1)–(A.4)) indicate the direction of force according to the Cartesian coordinate system of Figure 9 (see also Figure 10). The limits of the integrals in question are defined by the entry and exit points of the slip circle given by the points A' and T, respectively.

The coordinates of the points of action of the resultant normal and driving force (Figure 10) are as follows:

$$y_N = \frac{\int N_{x,i} y \mathrm{d}y}{\int N_{x,i} \mathrm{d}y} = \frac{\int W_i(y) \sin \omega_i \cos \omega_i y \mathrm{d}y}{\int W_i(y) \sin \omega_i \cos \omega_i \mathrm{d}y} \tag{A.9}$$

$$x_N = \frac{- \int N_{y,i} x \mathrm{d}x}{- \int N_{y,i} \mathrm{d}x} = \frac{\int W_i(x) \cos^2 \omega_i x \mathrm{d}x}{\int W_i(x) \cos^2 \omega_i \mathrm{d}x} \tag{A.10}$$

$$y_F = \frac{- \int F_{x,i} y \mathrm{d}y}{- \int F_{x,i} \mathrm{d}y} = \frac{\int W_i(y) \sin \omega_i \cos \omega_i y \mathrm{d}y}{\int W_i(y) \sin \omega_i \cos \omega_i \mathrm{d}y} \tag{A.11}$$

$$x_F = \frac{- \int F_{y,i} x \mathrm{d}x}{- \int F_{y,i} \mathrm{d}x} = \frac{\int W_i(x)(1 - \cos^2 \omega_i) x \mathrm{d}x}{\int W_i(x)(1 - \cos^2 \omega_i) \mathrm{d}x} \tag{A.12}$$

DOI: 10.1002/nag

It may be noted that as all components of the normal and driving forces given by Equations (A.1)–(A.4) are generated by the gravitational weight of the sliding mass, which is obviously vertical, the following equations must be satisfied:

$$N_{R,x} + F_{R,x} = 0 \tag{A.13}$$

$$N_{R,y} + F_{R,y} = W \tag{A.14}$$

Substituting Equations (A.1)–(A.4) into Equations (A.13) and (A.14), it can easily be shown that both preconditions are true. Moreover, from Equations (A.9) and (A.11), it is observed that the points of action of the resultant normal and driving force have the same $y-$coordinate, that is, $y_N = y_F$.

Finally, taking only into account, for the sake of brevity, the weighting force of the sliding mass through the equations given in this Appendix (Equations (A.1)–(A.4)) and the buoyancy force U, the safety factor expression of Equation (A.15) is obtained. For the cohesion and buoyancy force, as well as for any possible external loading, it stands for what it has been written in the main text.

$$FS_M = \frac{rc'L + r\gamma_s\left(|N_{R,y}|\sin\delta_1 + |F_{R,y}|\sin\delta_2\right)\tan\varphi' - rU\tan\varphi'}{r\gamma_s\left(|N_{R,y}|\cos\delta_1 + |F_{R,y}|\cos\delta_2\right)} \tag{A.15}$$

It is noted that Equation (A.15) always gives exactly the same safety factor values as Equation (3).

ACKNOWLEDGEMENTS

The authors wish to acknowledge the support of (i) NSF grant CMMI-0970122 on 'GOALI: Probabilistic Geomechanical Analysis in the Exploitation of Unconventional Resources' and (ii) KGHM Cuprum, Wrocław, Poland through the Framework 7 EU project on 'Industrial Risk Reduction' (IRIS).

NOTATION

c'	Cohesion with respect to effective stresses in kN/m^2
$d\alpha$	Infinitesimal angle in radians
ds	Infinitesimal length along the slip arc in meters
E_i	Interslice force acting parallel to $x-$axis in kN
E_v and E_h	Vertical and horizontal components of seismic force, respectively, in kN/m
FS_M	Safety factor of slope with respect to moment equilibrium
FS_F	Safety factor of slope with respect to force equilibrium
F_c	Force due to cohesion (resultant) in kN/m
F_d	The tangential component of W on the slip surface
F_φ	Friction force (resultant) in kN/m
F_u	Friction force due to the pore pressure force U ($F_u = U\tan\varphi'$) in kN/m
F_f	Footing force (concentrated loading) in kN/m
$F_{d,i}$	The tangential component of W_i
$F_{x,i}$ and $F_{y,i}$	The $x-$component and $y-$ component of $F_{d,i}$, respectively
$F_{R,x}$ and $F_{R,y}$	The $x-$component and $y-$ component of the resultant driving force of the sliding mass, respectively
$f_i(x)$ or $f_i(y)$	Mathematical functions representing the geometric elements of the problem (e.g., slope face and upslope area)
$f_{circ}(x)$ or $f_{circ}(y)$	The function of critical slip circle as for x and y
$f_u(x)$	The distribution function of pore pressures along the slip circle
$g_i(x)$	Mathematical function representing the interface between two successive soil layers

DOI: 10.1002/nag

H	Slope height in meters
H_w	Pool height in meters
h	Height of lower layer in a two-layer system measured from slope toe in meters
L	Length of slip circle in meters
M_f *and* M_d	Sum of the resisting and driving moments respectively in kNm
N_φ	The normal component of W on the slip surface
$N_{\varphi,i}$	The normal component of W_i
$N_{x,i}$ *and* $N_{y,i}$	The $x-$component and $y-$component of $N_{\phi,i}$, respectively
$N_{R,x}$ *and* $N_{R,y}$	The $x-$component and $y-$component of the resultant normal force of the sliding mass, respectively
r	The radius of the slip circle in meters
$\tan\beta$	Slope gradient
$u(x)$	Function representing the pore pressure distribution along the slip circle
U	Pore pressure force (resultant $U=\Sigma u$) in kN/m
V_T *and* V_p	Force due to water in tension crack and poor surcharge, respectively (concentrated loading) in kN/m
W	Weight of the sliding mass in kN/m
W_i	Weight of slice in kN
X_i	Interslice force acting parallel to $y-$axis in kN
x_C *and* y_C	The $x-$coordinate and $y-$coordinate, respectively, of the center of the failure mass in meters
$x_{C'}$ *and* $y_{C'}$	The x and y coordinates, respectively of the center of mass of the area bounded between the slip circle and the free water surface in meters
x_N *and* x_F	The $x-$coordinate of the resultant normal and driving force of the sliding mass, respectively
y_N *and* y_F	The $y-$coordinate of the resultant normal and driving force of the sliding mass, respectively
α_i *and* α_f	Angular position of the entry and exit point of slip circle with respect to the rotating center O, in radians
γ_s *and* γ_w	Specific gravity of soil and water, respectively, in kN/m^3
δ	Angle of inclination of the line passing through the center of the circle O and the point of projection of W on the slip surface
δ_1	Angle of inclination of the line passing through the center of the circle O and the point of projection of $N_{R,y}$ on the slip surface
δ_2	Angle of inclination of the line passing through the center of the circle O and the point of projection of $F_{R,y}$ on the slip surface
σ	Total normal stress in kN/m^2
σ'	Effective shear strength in kN/m^2
φ'	Friction angle of soil material with respect to effective shear stresses in degrees
ω_i	Angle defined by the direction of $N_{\phi,i}$ and the vertical

REFERENCES

1. Hatvin S. Grusfyllningar för kajbyggnader. *Teknisk Tidskrift* 1916; **46**:292.
2. Petterson KE, Kajraset I. Goteborg des 5 te Mars 1916. *Teknisk Tidskrift* 1916; **46**:289.
3. Petterson KE. The early history of circular sliding surfaces. *Geotechnique* 1955; **5**:275–96.
4. Fellenius W. *Erdstatische Berechnungen mit Reibung und Kohäsion (Adhäsion) und Unter Annahme Kreiszylindrischer Gleitflächen*. Ernst & Sohn: Berlin, 1927.
5. Fellenius W. Calculations of the stability of earth dams. In: Trans. of the 2nd Congress on Large Dams (Vol.4), Washington, D.C, 1936; p. 445–463.
6. Bishop AW. The use of the slip circle in the stability analysis of slopes. *Geotechnique* 1955; **5**:7–17.
7. Janbu N. Slope stability computations. Institutt for Geotknikk og Fundamenteringslære, Norges Tekniske Høgskole. Soils Mechanics and Foundation Engineering, the Technical University of Norway, 1968.
8. Lowe J, Karafiath L. Stability of earth dams upon drawdown. In: Proc of the First PanAmerican Conference on Soil Mechanics and Foundation Engineering. Mexico DF: Mexican Society of Soil Mechanics, 1960; p. 537–552.

DOI: 10.1002/nag

9. Morgenstern NR, Price VE. The analysis of the stability of generalised slip surfaces. *Geotechnique* 1965; **15**:79–93.
10. Spencer E. A method for analysis of the stability of embankments assuming parallel interslice forces. *Geotechnique* 1967; **17**(1):11–26.
11. Corps of Engineers. *Stability of earth and rock-fill dams*. EM 1110-2-1902. U.S. Army Engineer Waterways Experiment Station: Vicksburg, MS, 1970.
12. Corps of Engineers. *Engineering and Design—Slope Stability Engineering Manual*. EM 1110-2-1902. U.S Army Corps of Engineers: Washington, DC, 2003.
13. Sarma SK. Stability analysis of embankments and slopes. *Geotechnique* 1973; **23**(3):423–33.
14. Duncan JM. State of the art: limit equilibrium and finite-element analysis of slopes. *Journal of Geotechnical Engineering* 1996; **122**(7):577–96.
15. Cheng YM, Lau CK. *Slope stability analysis and stabilization: new methods and insight*. Taylor & Francis: New York, 2008.
16. Chen ZY, Morgenstern NR. Extensions to the generalized method of slices for stability analysis. *Canadian Geotechnical Journal* 1983; **20**:104–19.
17. Janbu N. Slope stability computations. In *Embankment Dam Engineering—Casagrande Volume*. John Wiley and Sons: New York, 1973.
18. Whitman RV, Bailey WA. Use of computers for slope stability analysis. *Journal of the Soil Mechanics and Foundations Division* 1967; **93**(SM4):475–98.
19. Duncan JM. Soil slope stability analysis. In *Landslides: Investigation and Mitigation*. Special Report No.247, Turner AK, Schuster RL (eds.). TRB: Washington, DC, 1996b; 337–371.
20. Duncan JM, Wright SG. *Soil strength and slope stability*. John Wiley and Sons: New York, 2005.
21. Fredlund DG, Krahn J. Comparison of slope stability methods. *Canadian Geotechnical Journal* 1977; **14**(3):429–39.

DOI: 10.1002/nag